Chemical Engineering Journal 499 (2024) 156574

Contents lists available at ScienceDirect

Chemical Engineering Journal

journal homepage: www.elsevier.com/locate/cej

3D printed photopolymer derived carbon catalysts for enhanced wet peroxide oxidation

Adriano S. Silva [a,b,c,d,*], Jose L. Diaz de Tuesta [e,**], Adriano Henrique [a], Fernanda F. Roman [a,b,c], Daria Omralinov [f], Hendryk Steldinger [f], Jan Gläsel [f,g], Bastian J.M. Etzold [f,g], Jose A.C. Silva [a], Adrián M.T. Silva [b,c], Ana I. Pereira [d], Helder T. Gomes [a]

[a] CIMO, LA SusTEC, Instituto Politécnico de Bragança, Campus de Santa Apolónia, 5300- 253 Bragança, Portugal.
[b] LSRE-LCM – Laboratory of Separation and Reaction Engineering – Laboratory of Catalysis and Materials, Faculty of Engineering, University of Porto, Rua Dr. Roberto Frias, 4200-465 Porto, Portugal
[c] ALiCE - Associate Laboratory in Chemical Engineering, Faculty of Engineering, University of Porto, Rua Dr. Roberto Frias, 4200-465 Porto, Portugal
[d] Research Centre in Digitalization and Intelligent Robotics (CeDRI), Instituto Politécnico de Bragança, Campus de Santa Apolónia, 5300-253 Bragança, Portugal
[e] Chemical and Environmental Engineering Group, ESCET, Universidad Rey Juan Carlos, c/Tulipán s/n, 28933 Móstoles, Spain
[f] Technische Universität Darmstadt, Ernst-Berl-Institut für Technische und Makromolekulare Chemie, 64287 Darmstadt, Germany
[g] Friedrich-Alexander-Universität Erlangen-Nürnberg, Power-to-X Technologies, Dr.-Mack-Str. 81, 90762 Fürth, Germany

ARTICLE INFO

Keywords:
3D-printing
Acetaminophen
Advanced oxidation processes (AOPs)
Contaminants of emerging concern (CECs)
Fenton-like
Metal-free monoliths

ABSTRACT

In this paper, we explore the application of powdered carbon and 3D-printed carbon monoliths prepared by carbonization of a tailored photopolymer. We demonstrate the efficiency of the developed carbonaceous samples in removing paracetamol (PCM) and sulfamethoxazole (SMX), used as model contaminants. Our results demonstrate that carbon samples are active in CWPO, and their catalytic activity is significantly improved by applying nitric acid and urea functionalization methods. The characterization results showed the pure carbon nature of the material (no ashes), their unique structure defects proven by Raman ($D/G > 1.8$), textural properties (S_{BET} = 291–884 m^2/g) and their surface chemistry, which was addressed by pH_{PZC} (2.5–7.5), acidity (312–2375 μ mol g_{cat}^{-1}) and basicity (117–653 μ mol g_{cat}^{-1}) determination and XPS of highlighted materials (N1s = 0–3.51 at.%, O1s = 7.1–15.3 at.%). Using desorption assays, our study reveals the adsorption role for pollutant degradation by CWPO using carbon monolithic samples. At last, we demonstrated the ability of functionalized 3D-printed carbon monoliths to keep degradation of PCM and total organic carbon (TOC) above 85 % and 80 %, respectively, during 48 h in a continuous flow CWPO system. Sulfamethoxazole degradation in continuous system was also studied to validate the catalyst versatility, achieving 81 % and 79 % pollutant degradation and TOC abatement, respectively, during 48 h on stream. The characterization of the recovered catalyst provides further insights into the absence of structural modifications after the reaction, reinforcing the stability and reusability characteristic of the 3D-printed carbon catalyst.

1. Introduction

The escalating challenges posed by rapid population growth, urbanization, and industrialization have intensified environmental concerns, particularly regarding the discharge of toxic compounds into water bodies [1–3]. Of particular concern are pharmaceutically active compounds (PhACs), such as acetaminophen (PCM) and sulfamethoxazole (SMX), which pose risks to aquatic life and human health [4,5]. The imperative for research in PhAC removal has spurred investigations into alternative wastewater treatment solutions, notably focusing on adsorption, membrane technologies, and advanced oxidation processes (AOPs) [6–10].

Catalytic wet peroxide oxidation (CWPO), or heterogeneous Fenton, using metal-free materials as catalysts offer promising solutions to the challenges faced by conventional Fenton and Fenton-like processes and other wastewater treatment technologies like adsorption, membrane

* Corresponding author at: Centro de Investigação de Montanha (CIMO), Instituto Politécnico de Bragança, Campus de Santa Apolónia, 5300-253 Bragança, Portugal.
** Corresponding author.
E-mail addresses: adriano.santossilva@ipb.pt (A.S. Silva), joseluis.diaz@urjc.es (J.L. Diaz de Tuesta).

https://doi.org/10.1016/j.cej.2024.156574
Received 17 June 2024; Received in revised form 2 September 2024; Accepted 8 October 2024
Available online 10 October 2024

filtration, and biological treatments [11–16]. Adsorption and membrane filtration primarily transfer pollutants from one phase to another without degrading them. In contrast, biological treatments, although effective, require extended operational times to achieve satisfactory pollutant conversion and fail for biological refractory compounds [17]. Fenton and Fenton-like reactions using metal-based materials suffer from several issues, such as leaching and formation of iron sludge, or it may require excess dose of H_2O_2 (*e.g.* copper-based catalysts) [18,19]. In addition, other Fenton-like processes such as photo-Fenton, sono-Fenton, and electro-Fenton reactions require additional infrastructure/cost to operate [20]. Hence, heterogeneous Fenton using metal-free materials can address these limitations by providing more efficient and effective pollutant degradation in wastewater treatment. However, challenges persist, particularly regarding catalyst activity and scalability for full-scale applications [21,22].

Materials with electron-donating groups available for H_2O_2 decomposition into oxidation radicals are often preferred for CWPO process [23]. Traditional catalysts used for this purpose are based on active phases supported on polymeric films [24,25], clays [26,27], zeolites [28], and carbon materials. Traditional carbon materials (*e.g.*, pyrochar, carbon black, among others) often lack heteroatoms on their surface, which makes them inert [23]. However, the presence of structural defects and/or functional groups (including oxygenated and nitrogenated groups) play a significant role in increasing the catalytic activity towards Fenton-like reactions [29,30]. Nevertheless, most carbon materials have residual metals, originating either from the precursor (*i.e.*, biomass [31]) or from the synthesis procedure (*i.e.*, chemical vapor deposition [32]), that may affect their activity in CWPO reaction. For this reason, it is rather difficult to understand the role of each phase (residual metal, carbon, and heteroatoms) in the activity of the carbon material. Polymer-derived activated carbons, synthesized from photopolymers, present a promising avenue for generating inorganic-free carbon materials with controlled properties [8,33]. Furthermore, most synthesis routes yield carbon materials in powder form, which would require additional steps to immobilize those particles for full-scale processes. Additive manufacturing, specifically 3D printing, arises as a suitable alternative to obtain three-dimensional rationally designed structures, enabling precise control over material structure and facilitating the obtention of architectures optimized for catalytic and adsorption applications [34]. Its application in water treatment is gaining attention for producing efficient catalytic structures [35], since structured catalysts are printed to minimize mass transfer limitations, improving radial and axial diffusion with low pressure drops under continuous flow operations.

For instance, 3D-printed metal–organic framework (MOF) coatings have shown high Rhodamine B degradation efficiency, and MOF-decorated ceramics have proven to be durable H_2O_2 activators, efficiently removing dyes and maintaining stability over multiple cycles [36]. Additionally, 3D printing can produce carbon structures with hierarchical porosity and precise morphological control, crucial for optimal catalytic performance. It allows for easier separation and recovery of catalysts from aqueous environments compared to traditional methods. In a previous work, a carbon monolithic structure synthesized by stereolithography (SLA) 3D printing demonstrated its potential application for the separation of alkane isomers [34]. Other works have also demonstrated the applicability of 3D-printed carbon materials for CO_2 adsorption [37], and ozonation [38]. However, the application of SLA 3D-printed metal-free carbon monoliths remains unexplored and represents one strategy to upgrade the feasibility of larger-scale quaternary wastewater treatment.

In this study, we propose the use of 3D-printed metal-free carbon monoliths as catalysts for CWPO, targeting the removal of PCM. The work involved a set of batch experiments with powdered carbon derived from these monoliths to assess the suitability of the materials, followed by functionalization studies to explore surface chemistry effects. Notably, our approach uses true photopolymer-derived metal-free carbon-based materials in CWPO, highlighting the intrinsic contribution of carbon in oxidation processes. Additionally, we delve into the role of adsorption in liquid-phase oxidation reactions and into the role of their surface chemistry changed by nitric acid and urea functionalization to elucidate their significance in CWPO processes. Furthermore, we present experimental findings from a continuous flow CWPO system, demonstrating the feasibility of employing functionalized 3D-printed carbon monoliths in dead-end mode operation, thus paving the way for scalable applications in wastewater treatment. The catalyst performance in removing organic pollutants was validated upon experiments for sulfamethoxazole (SMX) degradation in continuous mode, in a similar setup and experimental conditions as the PCM experiment.

2. Methodology

2.1. Reagents

Pentaerythritol tetraacrylate (PETA, containing 10–40 % triacrylate, 350 ppm hydroquinone) and divinylbenzene (DVB, containing 20 % ethylstyrene, 1000 ppm p-*tert*-butylcatechol), used as monomers in resin, were purchased from Sigma Aldrich and used without extracting the stabilizer. The dye agent Sudan 1 (≥95 %) and the initiator phenylbis(2,4,6-trimethylbenzoyl) phosphine oxide (BAPO, 97 %) were also purchased from Sigma Aldrich. The reagent used as porogen, bis(2-ethylhexyl) phthalate (≥98 %), was bought from Alfa Aesar. Nitric acid (65 wt%) and urea (65 wt%) used to modify the carbon samples were obtained from Riedel–de-Haën. Paracetamol (98 wt%, Alfa Aesar), sulfamethoxazole (>98 wt%, Supelco), hydrogen peroxide (30 % w/v, Fischer Chemical), titanium (IV) oxysulfate (99.99 % w/v, Sigma Aldrich), sulfuric acid (98 % v/v, Labkem), sodium sulfite (98 wt%, Panreac), acetonitrile (99.9 % v/v, Fisher Scientific), formic acid (98 %, Labkem), and orthophosphoric acid (85 % v/v, Fisher Chemical) were used in CWPO runs and in analytical techniques. Ethanol (99.8 % v/v, Fischer) and sodium hydroxide (98 %, Labkem) were used for desorption experiments. All compounds were used as received, *i.e.,* without further purification, and ultrapure water was employed in the solutions along the work.

2.2. Synthesis of monoliths

The synthesis involved 3D-printing a photoresin using stereolithography technology and subsequent carbonization following optimized conditions established in a previous work [33]. The photoresin comprised monomers (pentaerythritol tetraacrylate and divinylbenzene), a porogen agent (bis(2-ethylhexyl) phthalate), a dye (Sudan-I), and a photoinitiator (BAPO). The structure chosen for the 3D printing is the tetragonal piece shown in Fig. 1. The monolith (length = 70 mm, diameter = 13.85 mm) is a reticular structure with tetragonal unit cells (5.7 × 5.7 mm) which consist of four crossed rods (r = 0.7 mm) tracing the diagonals of the cube unit cell (*ca.* 70.6 % and 69.3 % of void fraction for unit cell and for monolithic structure, respectively), as in a previous work [34]. Printing was conducted on a Kudo Titan 2HR 3D-printer under specified conditions (see Table S1). The printed part (Figure S1a) underwent Soxhlet extraction with acetone for 24 h to remove the dye, followed by overnight drying at 60 °C (Figure S1b). Subsequently, oxidative stabilization was performed in air at 300 °C for 6 h (544 mL h^{-1}) with a heating rate of 10 °C min^{-1}, followed by thermal treatment under inert atmosphere at 900 °C for 0.3 h (10 NL h^{-1}) with a heating rate of 3.3 °C min^{-1}. The resulting material was named M1. Activation with CO_2 at 860 °C for 6 h (30 NL h^{-1}) with a heating rate of 10 °C min^{-1}, yielded material M2. Figure S2 brings an overview of the printed carbon monoliths.

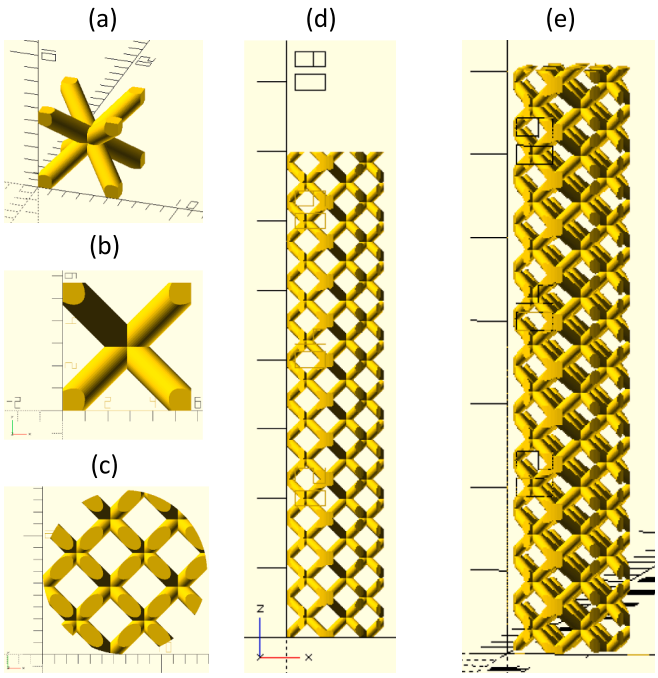

Fig. 1. Tetragonal unit monolith STL file used for printing carbon materials as view in OpensCAD software. Orthogonal projections for (a) diagonal view of the unit cell, (b) front view of the unit cell, (c) superior view of the monolith, (d) front view of the monolith, and (e) diagonal view of the monolith.

2.3. Sample conditioning, surface modification and characterization techniques

To ensure accurate assessment of catalytic activity, batch oxidation experiments of the target pollutant were conducted using carbon samples in powder form to mitigate internal and external diffusion limitations. For this purpose, the 3D printed samples (M1 and M2) were ground into powder and separated by particle size into different fractions (<53 μm, 53 < D < 106 μm, 106 < D < 160 μm, and > 160 μm). The ground and separated fractions were named according to particle size, with samples within the range 53 < D < 106 μm designated as M1_53:106 and M2_53:106, and those with particle size D > 160 μm named M1_160 and M2_160. Other particle size fractions were not used in this study.

Surface modification treatments were performed to evaluate changes in catalytic activity for removal of the organic pollutant by CWPO, following methodologies described elsewhere [39]. Acid treatment was conducted to enhance hydrophilicity by introducing surface oxygen groups. Ground carbon monoliths with granulometry 53 < D < 106 μm (M1_53-106 and M2_53-106) underwent boiling in a 5 M nitric acid solution at 120 °C for 3 h. The resulting materials, washed with distilled water and dried, were named M1A and M2A, respectively.

Another surface modification involved hydrothermal treatment of M1A and M2A samples with urea to introduce nitrogen groups and reduce acidity. The materials resulting from the acid treatment (M1A or M2A) were contacted with a 1 M urea solution at 200 °C for 2 h in a digestion vessel equipped with a removable PTFE cup (Model 4748 large capacity acid digestion vessel, Parr Instrument Company). The recovered solids, washed with distilled water and dried, were named M1AU and M2AU, respectively. The summary of material names, sizes, and surface modifications is provided in Table 1.

Characterization techniques were carried out following the methodology reported in previous works [40–42]. In summary, we conducted various analyses, including physisorption, thermogravimetric analysis (TGA) in air and nitrogen atmosphere, proximate and ultimate analysis, pH-drift method to determine pH_{PZC}, a simplified Boehm titration to assess acidity and basicity, Fourier-transform infrared (FTIR) spectroscopy and Raman spectroscopy for all samples. M2 materials were further characterized by X-ray photoelectron spectroscopy (XPS) [43]. The detailed description can be found in Text S1 on the Supplementary Materials.

Table 1
Sample names, particle sizes, and surface modifications.

Nomenclature	Size	Surface modification
M1_53:106	53 μm < D < 106 μm	No
M2_53:106	53 μm < D < 106 μm	No
M1_160	D > 160 μm	No
M2_160	D > 160 μm	No
M1A	53 μm < D < 106 μm	Nitric acid
M2A	53 μm < D < 106 μm	Nitric acid
M1AU	53 μm < D < 106 μm	Nitric acid and urea
M2AU	53 μm < D < 106 μm	Nitric acid and urea

2.4. Pollutants removal experiments

2.4.1. Batch runs of PCM degradation

CWPO experiments were conducted in a two-necked round bottom flask with 100 mL of model pollutant solution adjusted to pH 3.5 using H_2SO_4 (0.5 M). The solution contained a model pollutant concentration of 100 μg mL^{-1} and was heated to 80 °C, chosen based on previous studies [26]. After adding the stoichiometric amount of H_2O_2 (472 μg mL^{-1}), calculated based on Equation (1), the system was stirred for 5 min. At $t = 0$, 0.25 g of powdered carbon catalyst (C_{cat} = 2.5 g/L) was added. Samples were withdrawn periodically (15, 30, 60, 120, 240, 360, 480, and 1440 min) to monitor H_2O_2, TOC, and PCM concentrations. Samples for PCM and TOC analysis were stored with Na_2SO_3 to halt the reaction. The catalyst was recovered by filtration, dried overnight at 60 °C, and stored in case of future reutilization experiments.

$$C_8H_9NO_2 + 21H_2O_2 \rightarrow 8CO_2 + HNO_3 + 25H_2O \quad (1)$$

H_2O_2 decomposition tests were conducted for 8 h under the same conditions as oxidation runs, without the pollutant present. Adsorption experiments were carried out with all materials for 24 h under the same conditions as oxidation, without H_2O_2. Desorption assays were performed using carbon samples recovered from adsorption and oxidation runs. The procedure followed optimized conditions and solvents for PCM desorption from carbonaceous materials [44]. In brief, the recovered carbon samples were washed with 2 mL of distilled water to remove unadsorbed PCM. Then, 30 mg of recovered samples were stirred in 20 mL of an aqueous solution (0.1 M NaOH + 20 v/v% absolute ethanol) for 4 h at room temperature. The liquid phase was filtered and stored for further analysis. The amount of PCM desorbed from the materials was determined using Equation (2),

$$PCM_{des} = \frac{[PCM] \cdot V}{m_{ads}} \quad (2)$$

in which *[PCM]* represents the PCM concentration (mg/L) determined using HPLC, V the volume (L) of the aqueous extractant solution used for the experiment, and m_{ads} the mass (g) of material used in the experiment. The percentage of PCM desorbed was calculated considering the amount of PCM adsorbed into the material during pure adsorption experiments. To validate desorption experiments, samples recovered from reaction media were analyzed by FTIR and TGA (in N_2 atmosphere) to identify possible pollutant grafting during oxidation reactions or even the possibility of oxygen groups being formed at the carbon's surface due to their oxidation. XPS was also performed in the best catalyst after three reutilization cycles to assess surface modification.

All batch experiments, namely CWPO, catalytic H_2O_2 decomposition, adsorption and desorption, were performed in triplicate. The reported values are the average value, calculated according to Equation

(3),

$$\overline{C_t} = \frac{\sum_{j=1}^{n} C_j}{n} \quad (3)$$

where $\overline{C_t}$ is the average relative concentration of the parameter of interest (PCM, H_2O_2 or TOC concentration) at time t, C_j is the concentration in run j for time t, and n is the total number of experimental runs (n = 3). The standard deviation (s_t) was calculated according to Equation (4),

$$s_t = \sqrt{\sum_{j=1}^{n} \frac{(C_j - \overline{C_t})^2}{n-1}} \quad (4)$$

in which C_j is the relative concentration in time t for each run j, $\overline{C_t}$ the average concentration in time t (calculated by Equation (3), and n the total number of experimental runs. The standard deviation was below 5 % for all experiments. Hydrogen peroxide consumption efficiency (η_{H2O2}) was calculated according to reported in previous studies [32], as shown in Equation (5),

$$\eta_{H_2O_2} = \frac{X_{TOC_{t=8h}}}{X_{H_2O_{2t=8h}}} \cdot 100 \quad (5)$$

where $X_{TOCt=8h}$ is the conversion of TOC after 8 h of reaction and $X_{H2O2t=8h}$ is the conversion of hydrogen peroxide after 8 h of reaction.

2.4.2. Continuous flow mode CWPO experiments

After evaluating the effects of functionalization on PCM removal in batch experiments, the most effective functionalization method was applied to a 3D-printed carbon monolith. Following previous protocols, the monolith was used to assess PCM degradation capacity in a continuous flow mode CWPO system, as shown in Figure S3 [45]. The system consisted of an HPLC pump, a recirculation bath, a condenser tube (used as a jacketed reactor), and a stirrer plate. Operating conditions mirrored those of batch experiments: a solution of 100 μg mL^{-1} PCM with pH adjusted to 3.5 and a stoichiometric amount of H_2O_2 for mineralization ($[H_2O_2]_0$ = 473 μg mL^{-1}) of PCM were used as the inlet solution. The recirculation bath temperature was set to 82 °C to achieve the desired temperature of 80 °C for the pollutant/oxidant mixture.

The monolith was packed using glass wool and beads, and a volumetric flow rate (Q) was set to 0.75 mL min^{-1}, resulting in a residence time of approximately 6 min. Sampling occurred at regular intervals over 48 h to assess degradation of PCM. Additionally, samples were withdrawn from the influent solution to monitor concentration changes. After the reaction, the monolith was recovered, washed, and dried. Possible desorption of PCM was studied using the recovered material and the same extractant solution used in batch experiments, with a desorption assay conducted for 6 h. The same operating conditions were used to evaluate the catalyst capacity to degrade SMX, including CWPO (pH = 3.5, T = 80 °C, [SMX] = 100 μg mL^{-1}, $[H_2O_2]_0$ = 443 μg mL^{-1}), adsorption, H_2O_2 decomposition, and desorption assays.

The conversions of PCM, SMX, H_2O_2, and TOC, were calculated according to Eq. (7),

$$X = \left(1 - \frac{F_{c,outlet}}{F_{c,inlet}}\right) \cdot 100\% \quad (7)$$

$F_{c,outlet}$ is the mass flow of the compound c in the reactor outlet, and $F_{c,inlet}$ is the mass flow of the compound c in the reactor inlet. The non-catalytic experiment was performed without the carbon monolith under the same operating conditions and bed voidage as the material used. The space time (τ) was calculated according to Equation (8), as described elsewhere [46],

$$\tau = \frac{W(g_{cat})}{F_{c,inlet}(\mu mol_c \cdot h^{-1})} \quad (8)$$

in which W is the mass of catalyst and F is the inlet molar flow rate of the micropollutant. Adsorption experiments and H_2O_2 decomposition experiments were performed using a solution without H_2O_2 and pollutants, respectively.

The analytical techniques used to quantify PCM, SMX, H_2O_2, TOC, and iron species in treated water are explained in Text S2 and Figure S4.

3. Results and discussion

3.1. Characterization of carbon materials

3.1.1. Textural properties

The results obtained for monolithic piece dimension and weight during the synthesis procedure and surface modifications are shown in Table S2. The N_2 adsorption–desorption isotherms obtained for the carbonaceous catalysts are shown in Figure S5. The isotherms revealed a similar curve for all samples, with a hysteresis loop typical of H4-type materials according to the current IUPAC classification [47] a composite of types I and II. The pronounced adsorption observed at low relative pressures is related to the filling of micropores. The textural properties determined for the carbonaceous samples are shown in Table 2.

The results for materials with distinct particle sizes (*i.e.*, between 53 and 106 μm, or bigger than 160 μ m) revealed that both carbonaceous samples, M1 and M2, have uniform pore size distribution and textural properties. Nonetheless, samples from pristine M2 appear to have better uniformity in pore size distribution since the properties differ by about 3.3 % for the different particle sizes. In contrast, samples from M1 have an absolute difference of 8.3 %. Both values were calculated based on the average decrease/increase in the sample with particle sizes higher than 160 μ m, when compared to the sample with smaller particle sizes.

The acid functionalization significantly decreased the surface area (S_{BET}) for both materials (22.2 % for M1A and 11.5 % for M2A prepared from M1 and M2, respectively). The results obtained for the micropore surface area (S_{mic}) revealed the same behavior as the observed for S_{BET}, indicating that acid functionalization had the same effect over the carbonaceous material. The observed decrease in these textural properties appear to be associated with the potential formation of oxygen-containing functional groups at the pore opening region, obstructing the entry of N_2 molecules [48] or the modification of the pore structure upon acid attack [49]. The highest decrease in micropore surface area obtained for sample M1A (*ca.* 30 %) compared to M2A (*ca.* 12 %) can be related to the stronger oxidation achieved in this sample due to the lower micropore volume [50]. In both materials, the urea functionalization was responsible for increasing the surface area compared to the previous sample (M1A and M2A), which is related to the development of mesopores [39]. The behavior is confirmed by an increase in the external surface area (S_{ext}) observed for M2AU and M1AU compared to the previous sample and even to the pristine materials (M1_53:106 and M2_53:106).

3.1.2. Thermogravimetric characterization and chemical composition

All samples underwent TGA analysis under air and N_2 atmospheres.

Table 2
Textural properties of all carbonaceous materials.

Sample	S_{BET} (m^2/g)	S_{ext} (m^2/g)	S_{mic} (m^2/g)	V_{mic} (mm^3 g^{-1})	V_{Total} (mm^3 g^{-1})	V_{mic}/V_{Total} (%)	W_{mic} (nm)
M1_53:106	374	33	341	185	303	61	3.55
M1_160	409	38	371	202	338	60	3.64
M1A	291	37	254	138	257	54	2.17
M1AU	418	31	387	211	332	64	2.18
M2_53:106	884	51	833	452	615	73	2.17
M2_160	869	45	824	448	592	76	2.17
M2A	782	48	734	399	547	73	2.17
M2AU	790	50	740	401	544	74	2.17

The results shown in Fig. 2 indicate consistent modifications across material groups, with similar mass loss profiles. Carbon samples exhibited three major mass loss centers under airflow, with temperatures detailed in Table S3: removal of adsorbed water (86–89 °C), desorption of oxygen surface groups (289–295 °C), and carbon combustion (580–640 °C) [51]. Above 700 °C, only ash remains, confirming the whole carbon structure due to the synthesis procedure. Under N_2 flow, parent samples displayed similar mass profiles regardless of particle size, indicating uniform chemical composition. Acid-modified samples exhibited higher mass loss and water adsorption, with additional peaks attributed to removing weak oxygen functional groups [39]. Urea functionalization reduced mass loss in the range 100–600 °C, suggesting removal of oxygen groups introduced during acid treatment and restoration of temperature values closer to the original samples [30].

The chemical composition of carbonaceous samples was analyzed through proximate and ultimate (CHNS organic elemental determination) analysis, as shown in Table 3. Proximate analysis from TGA results in inert and air atmospheres (*cf.* Fig. 2) revealed similar results for the pristine samples M1 and M2, supporting sample homogeneity. Acid and urea modifications led to increased moisture content, likely due to an increase in hydrophilic characteristics of the materials. Treatments with acid and urea also increase the content of volatile matter (VM) observed in modified samples that can be associated to the surface functional groups (*ca.* 46.7 and 24.1 wt% of increment for samples prepared from M1 and *ca.* 22.4 and 23.8 wt% of increment for samples prepared from M2 monolith after acid and urea modifications, respectively). Treatment with urea reduced VM content compared to acid treatment (*ca.* 60.8 and 43.4 wt% for samples M1A and M2A *vs.*38.2 and 33.8 wt% for M1AU and M2AU samples), aligning with previous studies [30]. Content of fixed carbon (FC) decreased in acid-modified samples (*ca.* 81.4 and 87.3 wt% for samples M1 and M2 *vs.* 28.7 and 38.1 wt% for samples M1A and M2A), but increased with urea treatment (*ca.* 28.7 and 38.1 wt% for samples M1A and M2A *vs.* 48.4 and 51.2 wt% for samples M1AU and M2AU) due to removal of surface functional groups. Results of ultimate analysis agreed with proximate analysis, showing similar trends in carbon content and FC. Acid modification increased nitrogen content (0.6 and 0.5 wt% of difference for M1A and M2A respect to the respective pristine materials), while treatment with urea further increased nitrogen (2.6 wt% of nitrogen difference between M1AU and M1A; and 2.1 wt% of nitrogen difference between M2AU and M2A) and decreased oxygen content. Sulfur content remained null. The results of acidity/basicity properties of the carbon material surfaces are shown in Table 4 (pH_{PZC} curves exhibited in Figure S6). Samples from M1 showed balanced acidity/basicity, and samples from M2 exhibited more acidic characteristics. This behavior is consistent with findings from the literature on the effect of CO_2 activation on carbon materials [52]. Acid modification increased acidity significantly, while urea treatment reduced acidity, aligning with previous studies [39].

3.1.3. Surface chemistry

FT-IR and Raman spectra were used to study the surface chemistry of all materials. Fig. 3 shows the identification of D and G bands in the Raman spectra of all materials, which are characteristic of carbon-based materials [53]. All samples presented the bands in the same region, the D-band located in the range 1269–1286 cm^{-1} and the G-band in the range 1518–1603 cm^{-1} (detailed information reported in Table S4). The D-band is located between 1300–1350 cm^{-1} in most carbon materials. The shift towards smaller wavenumber has been associated with the highly disordered characteristic of carbon materials, indicating that all materials used in this work possess many defects in their structure [54]. The G band is associated with the presence of graphitic carbon (sp^2) and crystallinity and is present in all samples with a signal weaker than the D band. The spectra were used to determine peak areas of D and G bands by deconvolution, and the peak area ratio between D/G bands was calculated for all samples (Table S4). The values were all higher than 1.8 for all materials, which is characteristic of samples with a high degree of disorganization. The intensity of the 2D (G') band is low or absent for all materials.

The results obtained on FT-IR analysis are shown in Figure S7. The results revealed the presence of bands at 3450 and 1384 cm^{-1}, attributed to the OH stretching vibration and bending from the adsorbed water [32,55]. The weak band at 1620 cm^{-1} present in all materials is ascribed to the vibrations of the C = C bond, and the band at 2926 cm^{-1} is related to the stretching vibration of C-H bonds in CH_2 groups [32]. The results obtained in XPS analysis of M2 materials are shown in Fig. 4a. As observed, oxygen content significantly increase as consequence of acid attack from 7.1 *at.*% of M2_53:106 sample to 15.3 *at.*% of M2A. Furthermore, the functionalization with nitrogen-containing groups is evidence because of the content between samples M2A and M2AU (0.8 and 3.5 *at.*%, respectively). The detailed information on atomic percentages and peaks deconvolutions of O1s and N1s is shown in Table S5 and Figs. S8-S9. The results confirmed the increase in nitrogen content due to surface modification with urea, totalizing 3.51 % content in M2AU. The deconvolution of oxygen peak revealed about the same amount of carbonyl and C-O in esters and anhydrides groups. On the other hand, a significant increase in hydroxyl groups after acid treatment was observed (44 % in M2_53:106 to 63 % in M2A). The N1s peak deconvolution in M2AU catalyst revealed a predominance of pyridinic (32 %) and pyridonic or pyrrolic (41 %) groups.

3.2. Adsorption and pure H_2O_2 decomposition experiments

The results of pure adsorption experiment (Figure S10) reveal varying PCM removal efficiencies over time for all materials. Samples derived from M1 exhibited removals ranging from 10.3 to 30.2 % after 8 h of contact time, while samples from M2 achieved complete removal within just 30 min, irrespective of particle size or functionalization treatment. This disparity in performance can be attributed to differences in textural properties and surface chemistry between M1- and M2-derived samples. Notably, CO_2 activation of M1 resulted in M2 materials with enhanced surface areas due to the development of micropores in the carbonaceous structure, as confirmed in textural properties results (Table 2). The higher surface area of M2 materials (782–884 m^2/g, whereas 291–418 m^2/g was obtained for M1 samples) leads to significantly higher adsorption capacities (100 % for M2 *vs.* 10.7–30.2 % for M1). Although a direct comparison based solely on surface areas suggests M1 samples may reach roughly half the adsorption capacities of M2 samples, pore size distribution and surface chemistry play crucial roles in influencing adsorption capacity. The correlation between adsorption capacities and S_{BET} is discussed in more detail in Text S3 and Figure S11.

Pure H_2O_2 decomposition experiment results are discussed in Text S4 and Figure S12 [32,56,57].

3.3. Catalytic wet peroxide oxidation of paracetamol

The PCM, H_2O_2, and TOC concentration profiles during CWPO runs are depicted in Fig. 5 for all carbonaceous materials investigated. Notably, all materials demonstrated high catalytic activity towards removal of PCM, achieving over 90 % pollutant removal after 24 h of reaction. In terms of H_2O_2 decomposition, all catalysts exhibited decomposition rates exceeding 80 % after 24 h, surpassing results obtained in non-catalytic runs (X_{H2O2} = 10 %). Compared to non-catalytic conditions (X_{PCM} = 13 %), carbonaceous catalysts enhanced pollutant removal by at least 82 % by the end of the CWPO test. The observed removal of PCM in the absence of a catalyst was attributed to H_2O_2 oxidant activity, degrading 13 % of PCM in 24 h. Additionally, TOC removal exceeded 62 % for all materials, contrasting with the TOC removal of 7 % achieved under non-catalytic conditions. The high catalytic activity of all carbonaceous samples is justified due to the presence of structure defects on the carbon surface, which is confirmed by Raman

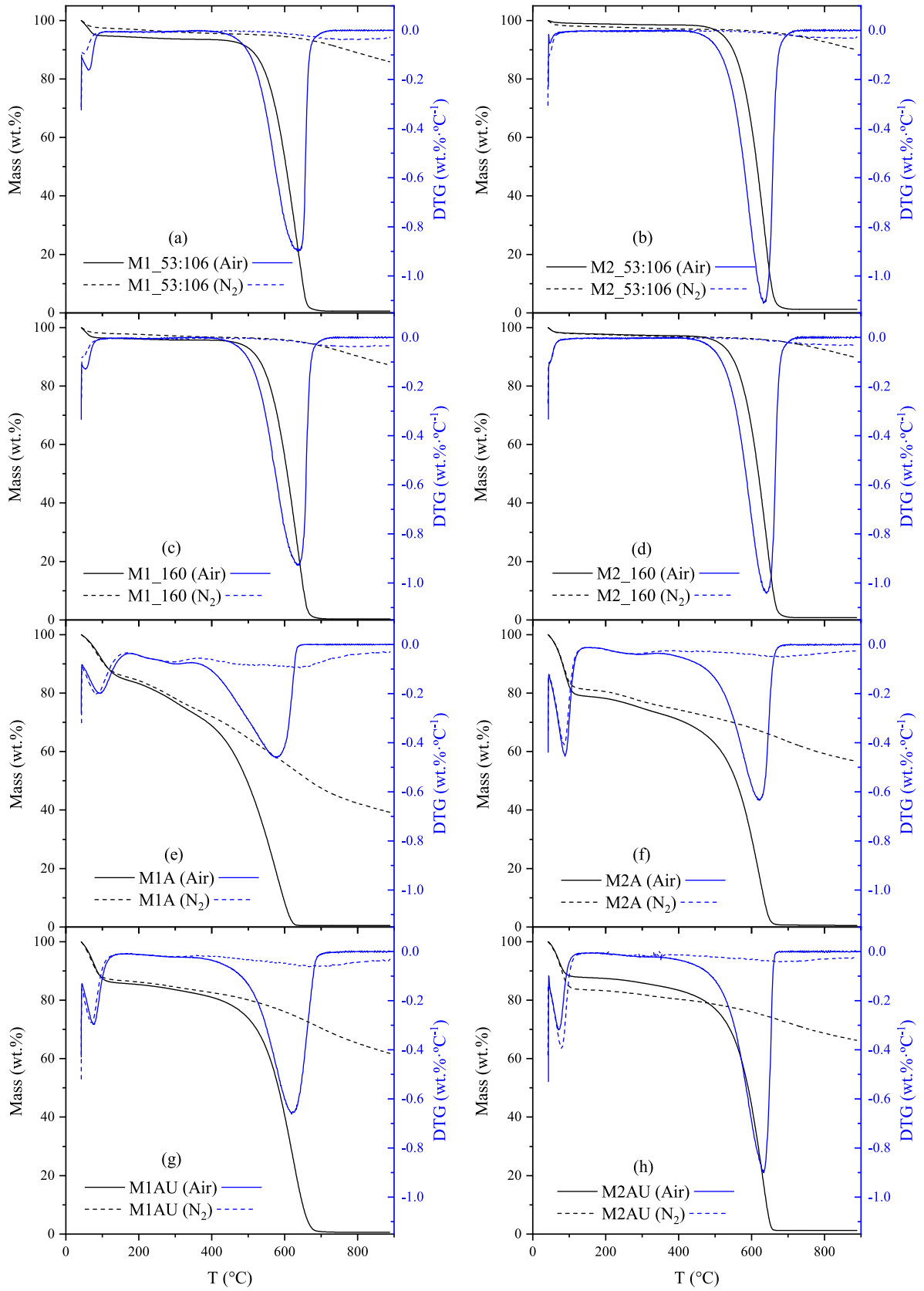

Fig. 2. TGA under air and nitrogen flow for (a-b) samples ground within 51–106 μm, (c-d) samples with particle size higher than 160 μm, (e-f) acid-treated samples, and (g-h) urea-thermal hydrotreated samples prepared from M1 and M2, respectively.

Table 3
Results of proximate and elemental analysis for all carbonaceous samples.

Sample	Proximate analysis*				Elemental analysis (dry basis)				Remaining** (*wt.%*)
	Moisture (*wt.%*)	VM (*wt.%*)	FC (*wt.%*)	Ash (*wt.%*)	C (*wt.%*)	H (*wt.%*)	N (*wt.%*)	S (*wt.%*)	
M1_53:106	3.9	14.1	81.4	0.6	86.9	0.7	<0.1	<0.1	11.8
M1_160	2.8	12.9	84.0	0.3	88.9	0.5	<0.1	<0.1	10.3
M1A	9.9	60.8	28.7	0.5	57.4	1.8	0.6	<0.1	39.7
M1AU	12.8	38.2	48.4	0.6	69.5	1.7	3.2	<0.1	25.0
M2_53:106	1.4	10.0	87.3	1.2	88.0	0.4	<0.1	<0.1	10.4
M2_160	2.0	10.3	86.9	0.8	87.7	0.4	<0.1	<0.1	11.1
M2A	17.9	43.4	38.1	0.6	63.5	1.7	0.5	<0.1	33.8
M2AU	13.8	33.8	51.2	1.2	64.8	0.7	2.6	<0.1	30.7

*Obtained from TGA under N_2 and air atmosphere as detailed in methodology; **Calculated as 100 – C (wt.%) – H (wt.%) – S (wt.%) – N (wt.%) – ashes (wt.%).

Table 4
pH_{PZC}, acidity and basicity of carbon materials.

Material	pH_{PZC}	Acidity (μmol g_{cat}^{-1})	Basicity (μmol g_{cat}^{-1})
M1_53:106	7.4	337	309
M1_160	7.5	312	296
M1A	2.7	2362	181
M1AU	6.5	1087	653
M2_53:106	6.9	425	143
M2_160	6.9	475	169
M2A	2.5	2375	117
M2AU	6.3	1112	576

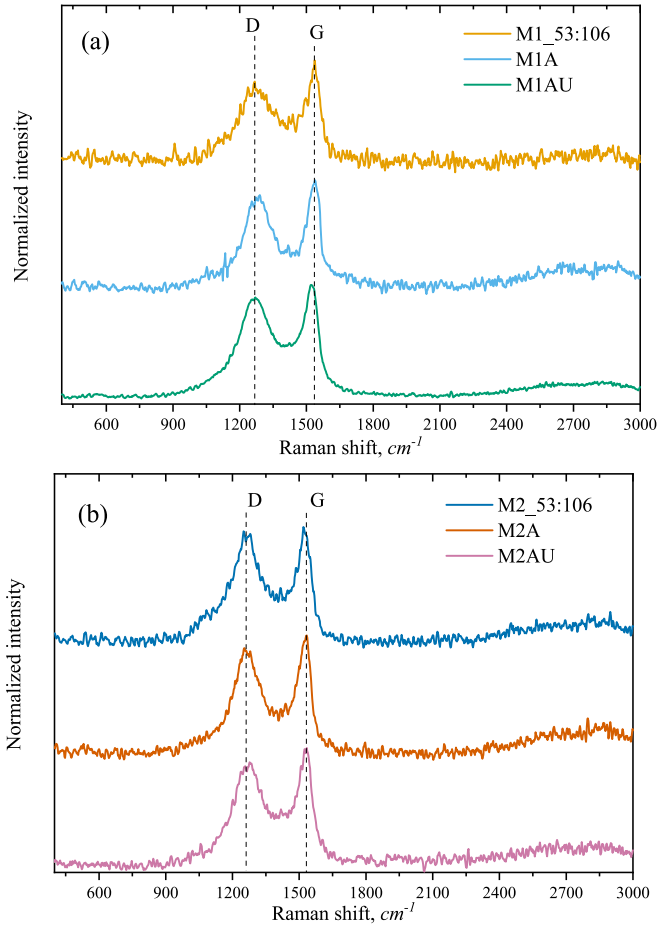

Fig. 3. Raman spectra for (a) samples prepared with M1 and (b) samples prepared with M2.

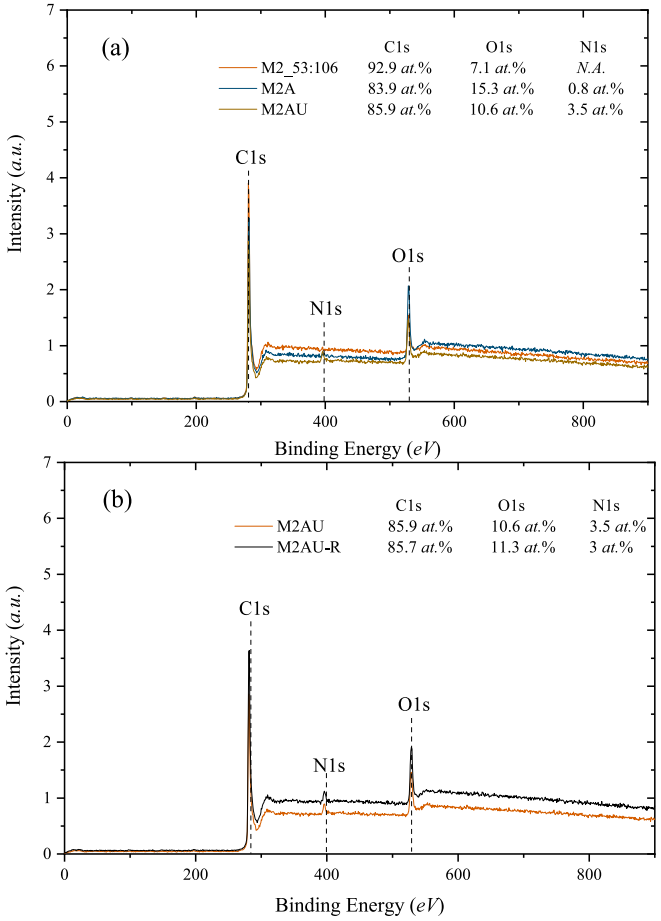

Fig. 4. XPS results obtained for (a) M2 materials and (b) comparison between fresh and reused M2AU catalyst.

results [58].

Comparison of pure H_2O_2 decomposition profiles with oxidant decomposition during CWPO experiments revealed similar trends for M1 materials. Acid functionalization facilitated a more controlled H_2O_2 decomposition profile, while urea functionalization improved oxidant decomposition. Conversely, materials M2 exhibited less pronounced H_2O_2 decomposition profiles, likely due to adsorption–desorption phenomena during oxidation reactions, partially hindering H_2O_2 access to active sites. Experiments with different particle sizes of M1 and M2 revealed varying catalytic performance. Despite diffusional limitations in larger particle sizes, both materials achieved similar PCM removal and H_2O_2 decomposition efficiencies. Notably, surface chemistry, rather than pore distribution, influenced catalytic performance. The influence of remaining content can be observed analyzing the materials before

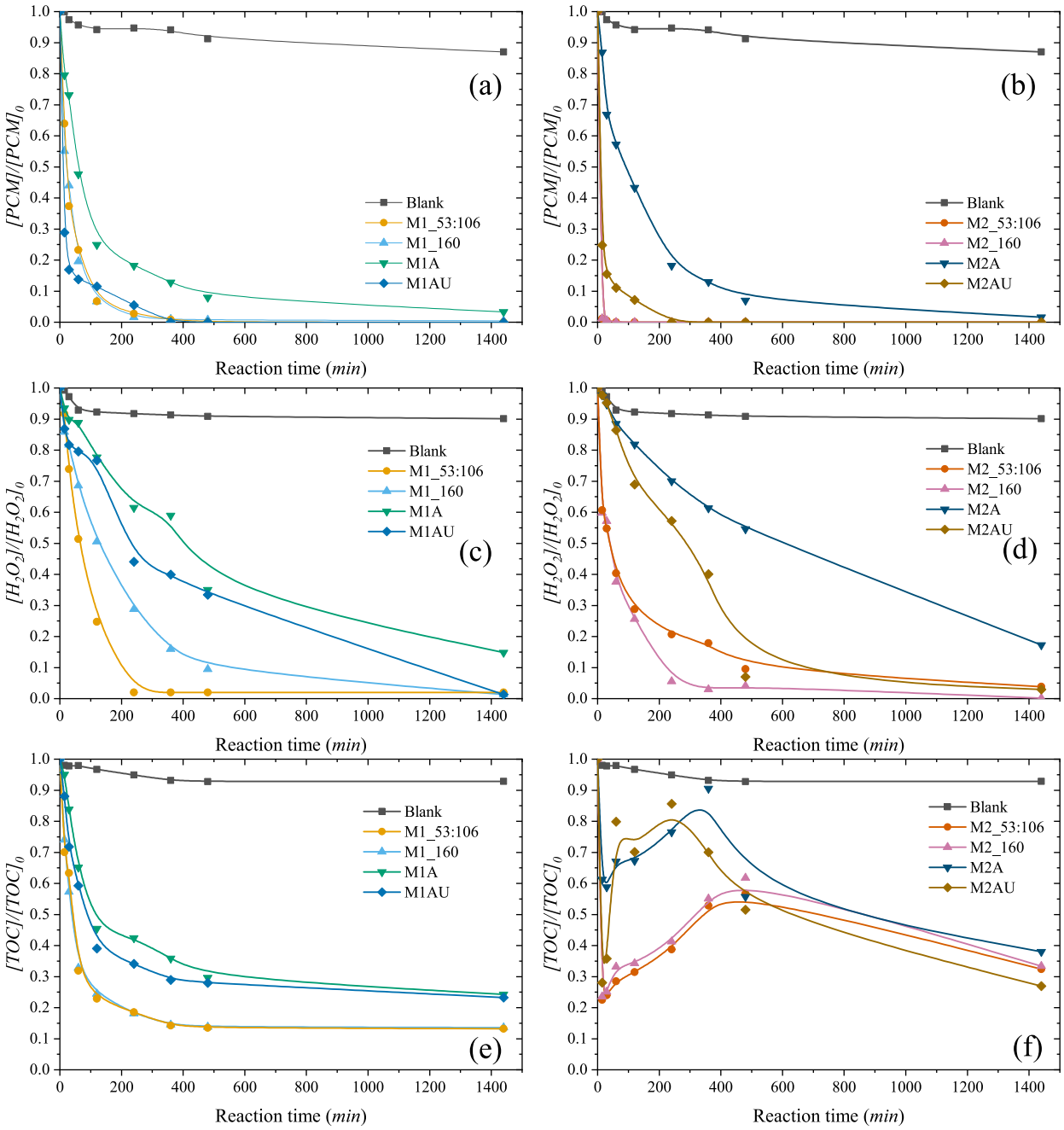

Fig. 5. Normalized concentration of PCM using catalysts prepared from materials (a) M1 and (b) M2; normalized concentration of H_2O_2 using (c) M1- and (d) M2-derived samples; and normalized concentration of TOC using catalysts prepared from samples (e) M1 and (f) M2 in CWPO experiments. Reaction conditions (batch): T = 80 °C, pH = 3.5, $C_{catalyst}$ = 2.5 g/L, $[PCM]_0$ = 100 μg mL^{-1}, $[H_2O_2]_0$ = 474 μg mL^{-1}. Lines are only intended to guide the eye.

urea functionalization. Figure S13 shows that H_2O_2 decomposition highly correlate (r^2 = 0.90) with the remaining content determined by elemental analysis (mostly oxygen) shown in Table 3.

Acid-functionalized samples exhibited diminished catalytic activity compared to pristine samples, attributed to decreased H_2O_2 decomposition rates and higher amount of acidic groups, as shown by acid/basic and pH_{PZC} characterization results (Table 4). However, acid-functionalized catalysts demonstrated more controlled H_2O_2 decomposition. Urea-functionalized catalysts showed improved activity, attributed to enhanced selectivity for hydroxyl radical generation. The result can be explained by the higher pH_{PZC} and amount of basic groups of urea-treated samples compared to acid functionalized and pristine samples [26]. The H_2O_2 decomposition after 24 h of reaction suggests a linear correlation between pH_{PZC} and amount of H_2O_2 decomposed (r^2 = 0.94), as shown in Figure S14. A comprehensive comparison of all materials is presented in Figure S15, considering parameters such as H_2O_2 decomposition efficiency and removal of PCM by adsorption and CWPO. Urea-functionalized carbon catalysts (M1AU and M2AU) exhibited the highest efficiency in H_2O_2 consumption, making them the most promising materials for the removal of PCM by CWPO. Previous works have shown that pyridinic nitrogen is associated with improved H_2O_2 decomposition [32], which is confirmed here with XPS results for M2AU (Fig. 4a and Table S5).

Furthermore, differences on PCM removal and H_2O_2 decomposition between samples M1 and M2 were attributed to increased microporosity in materials M2. Notably, samples M2 exhibited a unique TOC removal profile, with an initial decrease followed by an increase, suggesting the influence of adsorption–desorption phenomena and onsite oxidation of

adsorbed pollutants. This behavior is related with the saturation of the carbon surface at the beginning of the reaction due to strong adsorption effect. The high concentration of pollutant on the active site enables higher catalytic activity, considering that the materials M2 still had active sites available for H_2O_2 conversion. The TOC increased again due to the intermediates release in the middle reaction times (120–360 min). While AOP studies typically prioritize oxidation over adsorption, the evaluation of adsorption's role in catalytic removal of the pollutant remains crucial for understanding overall process contributions.

3.3.1. *Unravelling the role of adsorption in the removal of PCM by CWPO*

While adsorption is often evaluated to highlight role of oxidation in AOPs [8,26], it is crucial to not overlook highly adsorptive materials for oxidation processes. Adsorptive interactions facilitate contact between the pollutant and the hydroxyl radicals at the catalyst surface. To ascertain whether removal of pollutant is primarily driven by adsorption or oxidation, additional experiments like the desorption of physically adsorbed molecules are necessary [45]. Recent literature suggests that pollutants might be grafted onto the catalyst surfaces after applying an AOP [59]. For this reason, the catalyst after CWPO was also characterized to confirm whether the pollutant remains on the surface at the end of process. The FT-IR obtained for samples recovered from the CWPO reaction showed no difference compared to the fresh one, confirming that PCM was not grafted onto the surface of the materials. The results are shown in Fig. 6. The TGA results under nitrogen atmosphere for recovered samples is shown in Figure S16. Pure carbon samples (M1_53:106 and M2_53:106) resulted in a slightly higher mass loss after CWPO than pristine samples, which could be related to moisture content. The absence of mass loss ascribed to PCM desorbed in samples is related to the low amount (1.8 mg_{PCM}/g_{cat} was the maximum recovered) adsorbed in materials' surface. It is also possible to conclude that no significant amounts of oxidized intermediates or products were adsorbed on catalysts.

Desorption experiments were conducted on samples recovered from pure adsorption experiments to validate the methodology. The results, depicted in Fig. 7b, show the percentage of PCM recovered from carbonaceous samples. Approximately 64 % of PCM was recovered from M1 materials, while M2 samples yielded around 78 % recovery. The higher efficiency in PCM recovery in M1 materials may be attributed to mass transfer mechanisms. Overall, the method proved effective in desorbing PCM from carbonaceous materials, indicating that physisorption is the main adsorption mechanism for PCM removal by adsorption using these samples.

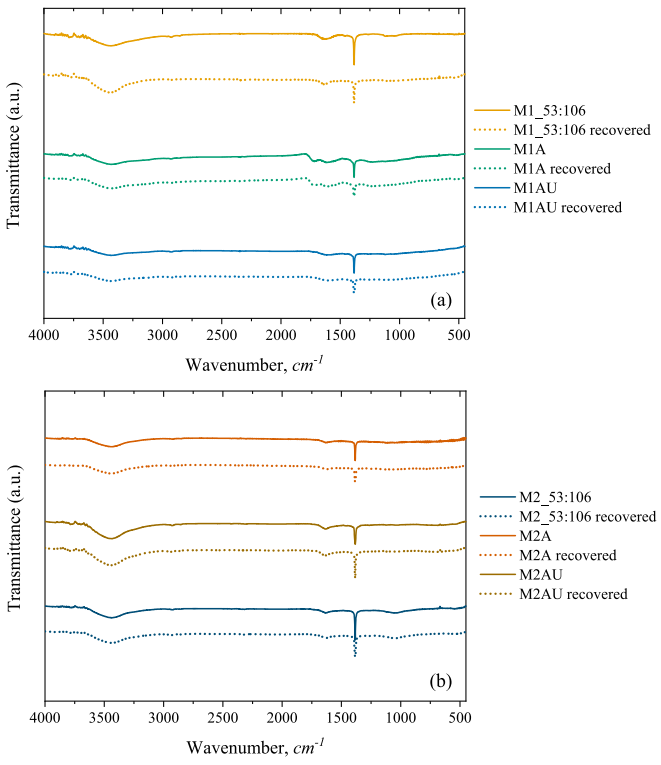

Fig. 6. Comparison between fresh and recovered materials from CWPO for catalysts (a) M1 and (b) M2 by FT-IR.

Desorption experiments using catalysts recovered from CWPO reactions (Fig. 7a) showed significantly less PCM compared to pure adsorption runs, indicating post-adsorption oxidation for all materials. This highlights the importance of desorption studies in understanding the role of adsorption in oxidation reactions. Comparison with pure adsorption trends revealed higher release of pollutant from pure carbonaceous samples, emphasizing the impact of adsorption capacities. Remarkably, catalysts M2 exhibited lower PCM release during desorption, suggesting onsite degradation and challenging assumptions about high adsorptive materials' suitability for CWPO.

Without desorption studies, conclusions on catalyst performance may be misleading. For example, despite higher adsorption capacities, materials M2 outperformed M1, confirmed by absent desorption of PCM in M2AU samples, indicating complete pollutant degradation during the reaction.

One of the main advantages of heterogeneous Fenton (or CWPO) reactions compared to the traditional homogeneous alternative is the possibility to recover the catalysts at the end of the reactions and reuse them. In some cases, the first use might be responsible for partial oxidation of the catalysts' surface, which can significantly impact the activity towards H_2O_2 decomposition and, consequently, the performance in pollutant removal. The results obtained for the reutilization runs after recovered and reused the best catalyst (M2AU) are shown in Fig. 8. The catalyst recovered after three cycles was analyzed by XPS, and the result is shown in Fig. 4b. As observed, oxygen content slightly increase from 10.6 to 11.3 *at.*% and nitrogen decreased from 3.5 to 3 *at.* %. The deconvolution results are shown in Figures S17-S18. The XPS result revealed a partial oxidation of the catalyst surface (carbonyl, hydroxyl, C-O, and carboxylic groups increased 11 %, 15 %, 8 %, and 7 %, respectively). On the other hand, the distribution of nitrogenated groups was not affected significantly. The results demonstrate that the catalyst maintained about the same activity in the second and third runs compared to the first run, confirming the potential application of this material in the studied process. The comparison with the literature dealing with batch PCM removal is available on Text S5 [8,26,60,61].

3.3.2. *Proof of concept: Continuous flow mode CWPO experiments*

The best catalyst, M2AU, was employed in a continuous flow mode CWPO experiment (dead-end) to assess PCM degradation capacity using the setup represented in Figure S3 (Figure S19 shows the reactor in operation). The mass and dimension of the printed monolith change during carbonization and functionalization processes as shown in Table S2. The resultant M2AU monolith has a weight, diameter and length of 0.40 g, 7.3 mm and 33 mm, respectively (82 % and 86 % of volume decrease from printed structure to carbonized and functionalized monolith, respectively). As the inlet stream was set at 0.75 $mL{\cdot}min^{-1}$, the space–time (τ) used for these experiments was 1.03 g_{cat} min $\mu mol_{PCM}{}^{-1}$, respectively.

Fig. 9a displays conversions of PCM, H_2O_2, and TOC. At the first collection point (1 h of time on stream), PCM removal reached 95.3 %, with an H_2O_2 conversion of 66 % and TOC removal of 24 %. Strong PCM adsorption likely contributed to this high removal, while low TOC conversion suggests possible on-site degradation of PCM and intermediate release. Hydroquinone, an identified intermediate, is quantified in Fig. 9b. After an initial period of reaction, a decline in H_2O_2 decomposition occurred at 2, 4, and 6 h on stream, attributed to pore blocking by oxidized organic intermediates. Competition for active sites among PCM, intermediates, and H_2O_2 ensued until reaching a steady state.

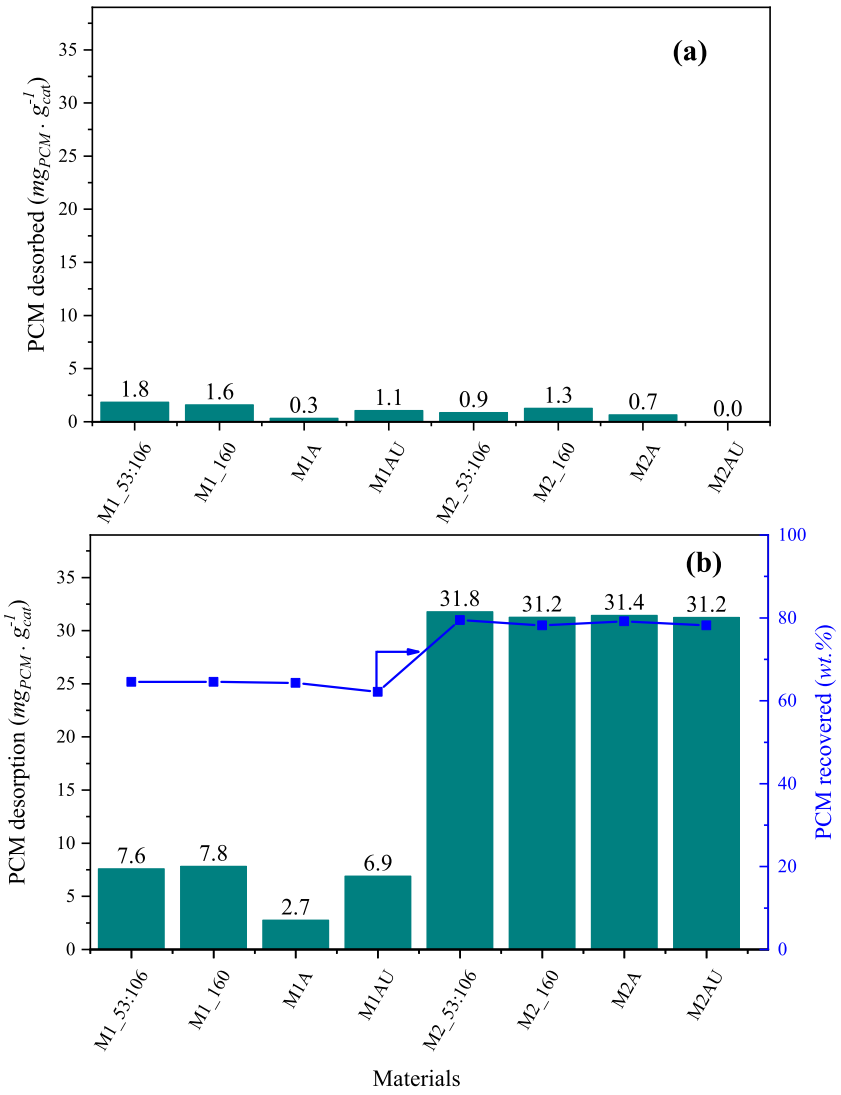

Fig. 7. (a) Desorbed PCM from catalysts recovered from CWPO experiments and (b) desorbed PCM from materials recovered from pure adsorption experiments.

Nevertheless, hydroxyl radicals decomposed sufficiently, elevating on-stream TOC conversion from 34.2 to 52.1 % from 4 to 6 h, respectively.

After 4 h on stream, H_2O_2 conversion increased, leading to more intermediates and decreased hydroquinone concentration, suggesting a possible TOC reduction. The continuous rise in TOC abatement over time may result from enhanced catalytic activity of the carbon materials, as observed previously with carbon black [62], or from oxidized intermediates acting as redox initiators to promote H_2O_2 decomposition and oxidation [63]. By 24 h, the reaction reached a steady state, achieving PCM degradation rates exceeding 93 %, TOC abatement up to 85 %, and over 96 % H_2O_2 decomposition over 48 h, with a space–time of 1.03 g_{cat} min μmol_{PCM}^{-1}. Notably, there are no reports in literature evaluating pure carbon materials as catalysts for degradation of organic pollutants using a similar technology. Previous studies achieved complete decomposition of H_2O_2 within 20 min, enabling full pollutant removal, albeit only for 3 h [45]. However, the catalysts used, magnetite-based, risk deactivation due to iron-phase composition. Another study explored activated carbon for metronidazole degradation using persulfate radicals, achieving up to 90 % degradation over 1.5 h but experiencing deactivation after 7 h [64]. Additionally, CNT-composite membranes demonstrated a removal of 70 % venlafaxine over 24 h in another study [65], although fouling can occur over time. The carbon monolith recovered from the reaction showed no significant alteration in mass (0.41 before reaction and 0.40 after reaction).

The H_2O_2 decomposition and adsorption experiments were performed to analyze the capacity of the best material, M2AU, to decompose H_2O_2 and evaluate the adsorption capacity. The results obtained are shown in Fig. 10a. The H_2O_2 decomposition experiments revealed a trend similar to the one observed in CWPO in all three cycles using the same monolith. The first cycle revealed slightly higher conversions than CWPO (>3%), which can be associated with the active site dispute between pollutant and oxidant over the reaction. The conversion of H_2O_2 obtained in the second and third experiments had about the same result as in the first experiment, which is different from what is commonly observed in the literature. In most cases, there is a higher loss of activity upon using the same material in cycles related to the oxidation of the material surface due to the contact with H_2O_2.

The result obtained for the pure adsorption experiment is shown in Fig. 10b. In the first 2 h of the experiment, the removal of pollutant by adsorption remained above 95 %, similar to the result obtained for CWPO in continuous mode. However, the adsorption of PCM dropped significantly to 7 % after 24 h and 0 % after 48 h. The result obtained for longer times of experiment is related to the PCM saturation at the material surface, hindering further adsorption of the pollutant. This result confirms the CWPO as the main removal mechanism during CWPO reactions, in which the PCM conversion was recorded above 85 % during the 48 h of experiment. The analysis of iron leached revealed that no iron was present in the aliquot recovered after 48 h of experiment.

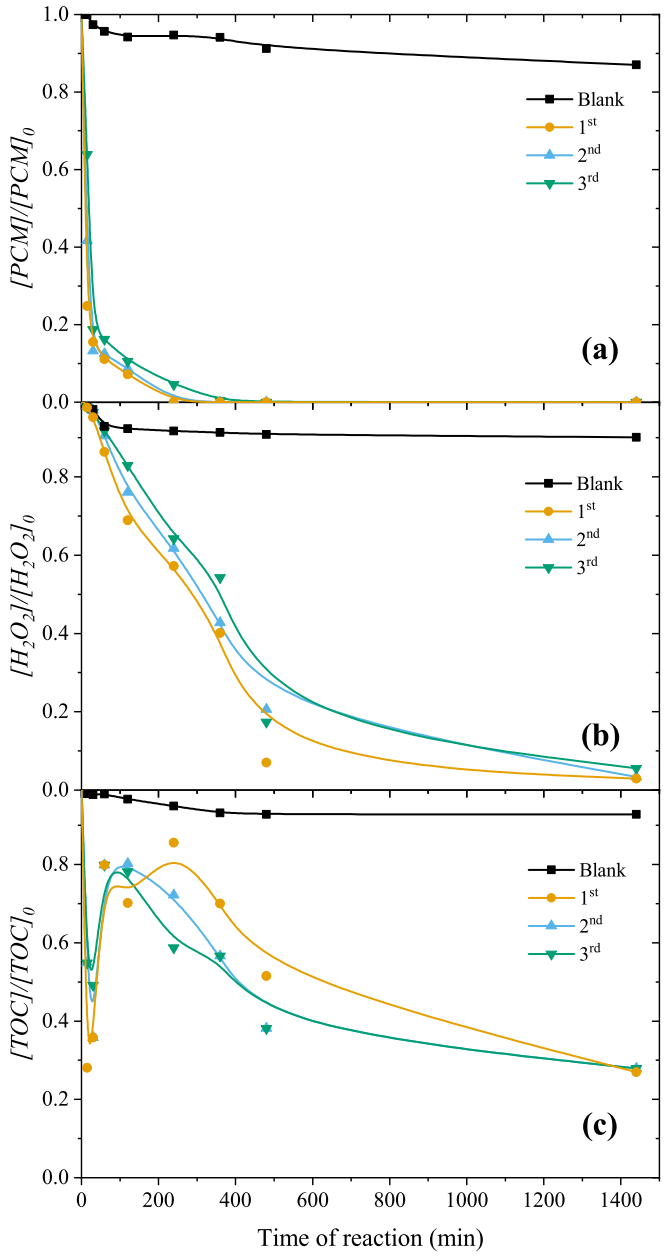

Fig. 8. CWPO reutilization experiments for catalyst M2AU. T = 80 °C, pH = 3.5, $C_{material}$ = 2.5 g/L, $[PCM]_0$ = 100 μg mL^{-1}, $[H_2O_2]_0$ = 474 mg/L. Lines are only intended to guide the eye.

The catalyst universal adaptability was assessed by performing a similar degradation experiment with another organic micropollutant, SMX in this case. The result obtained for H_2O_2 decomposition, SMX degradation, and TOC abatement are shown in Figure S20a. The results confirmed the catalytic performance of the material since SMX degradation, H_2O_2 decomposition, and TOC abatement achieved the steady state 24 h on with 81 % SMX degradation, 78 % H_2O_2 decomposition, and 80 % TOC abatement. The lower H_2O_2 conversion observed here compared to the results obtained with PCM is related to the higher SMX adsorption capacity of the monolith, increasing the competitiveness of the active sites. Still, the system kept high SMX degradation and TOC abatement once steady state was achieved. The adsorption experiment revealed the material was saturated with 24 h (Figure S20b), proving the catalytic removal over adsorption.

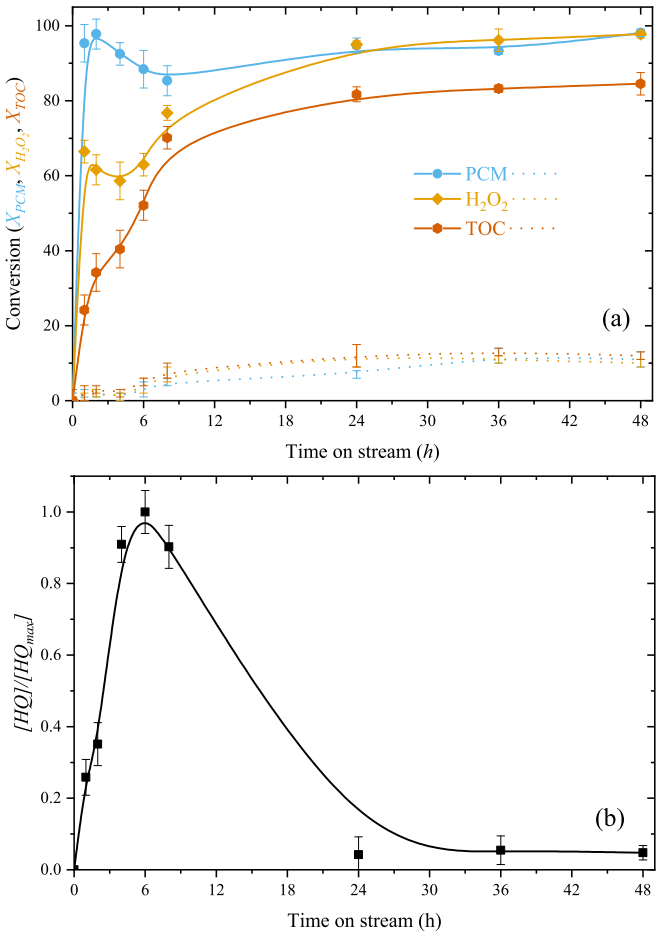

Fig. 9. (a) Results of continuous CWPO. T = 80 °C, pH = 3.5, $[PCM]_0$ = 100 μg mL^{-1}, $[H_2O_2]_0$ = 474 mg/L, Q = 0.75 mL min^{-1}. Dot lines represent non-catalytic results. (b) Normalized concentration of hydroquinone (HQ) over continuous CWPO experiment. Lines are only intended to guide the eye. (Not identified during non-catalytic run). Lines are only intended to guide the eye.

4. Conclusions

The carbon material samples obtained from crushing carbon monolith synthesized via stereolithography 3D printing demonstrated high catalytic activity in the degradation of PCM by CWPO. The functionalization changed the chemical and textural properties of the original carbon materials, increasing the catalytic activity of the carbonaceous materials upon urea functionalization. The traditional route for comparing the activity of different catalysts generally considers that materials with very strong adsorption capacities would not be so good for catalytic purposes. In the present study, the desorption experiments performed with materials recovered from both pure adsorption runs and CWPO reactions were fundamental for judging the most efficient material. For instance, if only pure adsorption results were considered, M2 materials (CO_2 activated) would be considered unsuitable for CWPO reactions since they possess high adsorption capacities due to their high surface area. In contrast, the desorption experiments revealed that M2 materials released less PCM during the desorption experiments compared to M1 materials, indicating that more pollutant was oxidized *in-situ*.

The results obtained for the removal of PCM in continuous CWPO experiments with 3D-printed carbon monolith functionalized with nitric acid and urea treatments revealed high stability and pollutant removal over the 48 h of experiment. In addition, the SMX degradation experiment in continuous mode confirmed the adaptability of the catalyst with another organic micropollutant. The result opens a variety of future

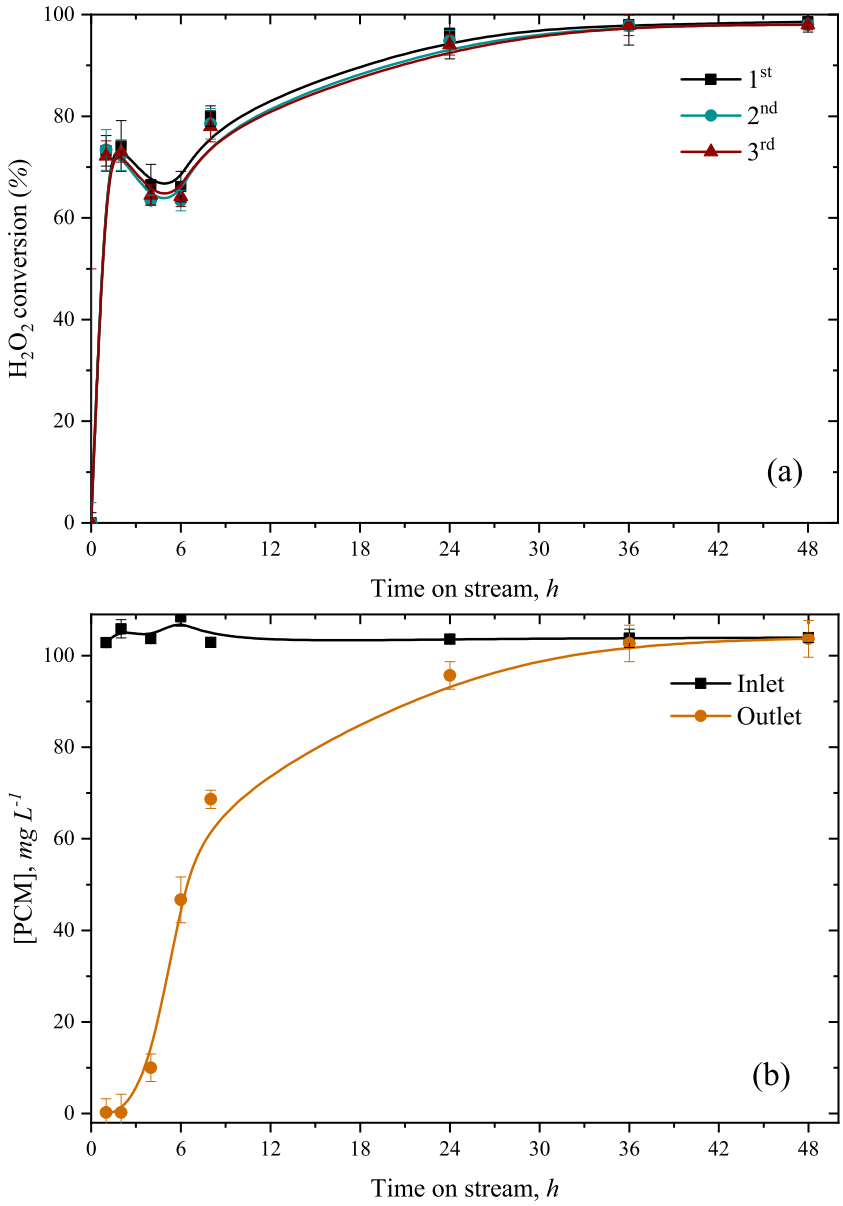

Fig. 10. (a) Cyclic H_2O_2 decomposition experiment in continuous mode and (b) adsorption experiment in continuous mode. Lines are only intended to guide the eye.

works to explore different monolithic shapes to evaluate improvements in catalytic degradation of pollutants or fluid circulation. Furthermore, the resin here presented could be further explored as template for the dispersion of metal-based materials, with applicability for environmental and energy purposes.

CRediT authorship contribution statement

Adriano S. Silva: Conceptualization, Formal analysis, Investigation, Methodology, Writing – original draft, Writing – review & editing. **Jose L. Diaz de Tuesta:** Writing – review & editing, Supervision, Project administration, Methodology, Funding acquisition, Conceptualization. **Adriano Henrique:** Investigation, Formal analysis. **Fernanda F. Roman:** Methodology, Writting – original draft, Investigation, Formal analysis. **Daria Omralinov:** Methodology, Investigation. **Hendryk Steldinger:** Methodology. **Jan Gläsel:** Writing – review & editing, Methodology, Conceptualization. **Bastian J.M. Etzold:** Writing – review & editing, Supervision, Project administration, Methodology, Funding acquisition, Conceptualization. **Jose A.C. Silva:** Writing – review & editing, Supervision, Methodology, Conceptualization. **Adrián M.T. Silva:** Writing – review & editing, Supervision, Funding acquisition. **Ana I. Pereira:** Writing – review & editing, Supervision, Funding acquisition. **Helder T. Gomes:** Writing – review & editing, Supervision, Project administration, Funding acquisition.

Declaration of competing interest

The authors declare that they have no known competing financial interests or personal relationships that could have appeared to influence the work reported in this paper.

Acknowledgments

The authors acknowledge the joint financial support from Fundação para a Ciência e a Tecnologia (FCT), in Portugal, and the Deutscher Akademischer Austauschdienst (DAAD), in Germany. This work was supported by national funds through FCT/MCTES (PIDDAC): CIMO, UIDB/00690/2020 (DOI: 10.54499/UIDB/00690/2020) and UIDP/00690/2020 (DOI: 10.54499/UIDP/00690/2020); and SusTEC, LA/P/0007/2020 (DOI: 10.54499/LA/P/0007/2020). This work was also

supported by national funds through FCT/MCTES (PIDDAC): LSRE-LCM, UIDB/50020/2020 (DOI: 10.54499/UIDB/50020/2020) and UIDP/50020/2020 (DOI: 10.54499/UIDP/50020/2020); and ALiCE, LA/P/0045/2020 (DOI: 10.54499/LA/P/0045/2020). Fernanda F. Roman acknowledges FCT and the European Social Fund (FSE) for the individual research grant with reference SFRH/BD/143224/2019. Adriano Silva was supported by the doctoral Grant SFRH/BD/151346/2021 financed by FCT with funds from NORTE2020, under MIT Portugal Program. Jose L. Diaz de Tuesta acknowledges the financial support through the program of *Atracción al Talento* of *Comunidad de Madrid* (Spain) for the individual research grant and project 2022-T1/AMB-23946.

Statement

During the preparation of this work the authors used ChatGPT in order to reduce the manuscript size and improve readability. After using this tool, the authors reviewed and edited the content as needed and take full responsibility for the content of the publication.

Appendix A. Supplementary data

Supplementary data to this article can be found online at https://doi.org/10.1016/j.cej.2024.156574.

Data availability

Data will be made available on request.

References

[1] E. Brillas, Fenton, photo-Fenton, electro-Fenton, and their combined treatments for the removal of insecticides from waters and soils. A review, Sep. Purif. Technol. 284 (2022) 120290, https://doi.org/10.1016/j.seppur.2021.120290.
[2] Y. Yang, H. Zhu, X. Xu, L. Bao, Y. Wang, H. Lin, C. Zheng, Construction of a novel lanthanum carbonate-grafted ZSM-5 zeolite for effective highly selective phosphate removal from wastewater, Microporous Mesoporous Mater. 324 (2021), https://doi.org/10.1016/j.micromeso.2021.111289.
[3] Y. Yang, D. Liu, Y. Chen, J. He, Q. Li, Mechanistic study of highly effective phosphate removal from aqueous solutions over a new lanthanum carbonate fabricated carbon nanotube film, J. Environ. Manage. 359 (2024), https://doi.org/10.1016/j.jenvman.2024.120938.
[4] S. Khan, Mu. Naushad, M. Govarthanan, J. Iqbal, S.M. Alfadul, Emerging contaminants of high concern for the environment: current trends and future research, Environ. Res. 207 (2022) 112609, https://doi.org/10.1016/j.envres.2021.112609.
[5] R.B. González-González, P. Sharma, S.P. Singh, J.H.P. Américo-Pinheiro, R. Parra-Saldívar, M. Bilal, H.M.N. Iqbal, Persistence, environmental hazards, and mitigation of pharmaceutically active residual contaminants from water matrices, Sci. Total Environ. 821 (2022) 153329, https://doi.org/10.1016/j.scitotenv.2022.153329.
[6] C.A. Sophia, E.C. Lima, Removal of emerging contaminants from the environment by adsorption, Ecotoxicol. Environ. Saf. 150 (2018) 1–17, https://doi.org/10.1016/j.ecoenv.2017.12.026.
[7] S. Kim, K.H. Chu, Y.A.J. Al-Hamadani, C.M. Park, M. Jang, D.-H. Kim, M. Yu, J. Heo, Y. Yoon, Removal of contaminants of emerging concern by membranes in water and wastewater: a review, Chem. Eng. J. 335 (2018) 896–914, https://doi.org/10.1016/j.cej.2017.11.044.
[8] J.L. Diaz de Tuesta, A.S. Silva, F.F. Roman, L.F. Sanches, F.A. da Silva, A.I. Pereira, A.M.T. Silva, J.L. Faria, H.T. Gomes, Polyolefin-derived carbon nanotubes as magnetic catalysts for wet peroxide oxidation of paracetamol in aqueous solutions, Catal. Today 419 (2023) 114162, https://doi.org/10.1016/j.cattod.2023.114162.
[9] J. Wang, B. Xiong, L. Miao, S. Wang, P. Xie, Z. Wang, J. Ma, Applying a novel advanced oxidation process of activated peracetic acid by $CoFe_2O_4$ to efficiently degrade sulfamethoxazole, Appl. Catal. B 280 (2021) 119422, https://doi.org/10.1016/j.apcatb.2020.119422.
[10] S. Saeid, P. Tolvanen, N. Kumar, K. Eränen, J. Peltonen, M. Peurla, J.-P. Mikkola, A. Franz, T. Salmi, Advanced oxidation process for the removal of ibuprofen from aqueous solution: a non-catalytic and catalytic ozonation study in a semi-batch reactor, Appl. Catal. B 230 (2018) 77–90, https://doi.org/10.1016/j.apcatb.2018.02.021.
[11] M. Priyadarshini, I. Das, M.M. Ghangrekar, L. Blaney, Advanced oxidation processes: performance, advantages, and scale-up of emerging technologies, J. Environ. Manage. 316 (2022) 115295, https://doi.org/10.1016/j.jenvman.2022.115295.
[12] J.J. Pignatello, E. Oliveros, A. MacKay, Advanced oxidation processes for organic contaminant destruction based on the Fenton reaction and related chemistry, Crit. Rev. Environ. Sci. Technol. 36 (2006) 1–84, https://doi.org/10.1080/10643380500326564.
[13] Y. Zhu, R. Zhu, Y. Xi, J. Zhu, G. Zhu, H. He, Strategies for enhancing the heterogeneous Fenton catalytic reactivity: a review, Appl. Catal. B 255 (2019) 117739, https://doi.org/10.1016/j.apcatb.2019.05.041.
[14] Y. Yang, Y. Wang, C. Zheng, H. Lin, R. Xu, H. Zhu, L. Bao, X. Xu, Lanthanum carbonate grafted ZSM-5 for superior phosphate uptake: investigation of the growth and adsorption mechanism, Chem. Eng. J. 430 (2022), https://doi.org/10.1016/j.cej.2021.133166.
[15] Y. Yang, R. Xu, C. Zheng, Y. Long, S. Tang, Z. Sun, B. Huang, J.P. Chen, Hierarchical hollow zeolite fiber in catalytic applications: a critical review, Chemosphere 307 (2022), https://doi.org/10.1016/j.chemosphere.2022.135899.
[16] B. Yuan, X. Huang, S. Yang, Y. Yang, Z. Lin, R. Semiat, J. Paul Chen, Development of a magnetic calcium-alginate hydrogel-sphere encapsulated with Fe–Mn–Zr ternary metal composite for heavy metal adsorption, Sep. Purif. Technol. 306 (2023), https://doi.org/10.1016/j.seppur.2022.122531.
[17] S. Rafaqat, N. Ali, C. Torres, B. Rittmann, Recent progress in treatment of dyes wastewater using microbial-electro-Fenton technology, RSC Adv. 12 (2022) 17104–17137, https://doi.org/10.1039/d2ra01831d.
[18] S. Hussain, E. Aneggi, D. Goi, Catalytic activity of metals in heterogeneous Fenton-like oxidation of wastewater contaminants: a review, Environ. Chem. Lett. 19 (2021) 2405–2424, https://doi.org/10.1007/s10311-021-01185-z.
[19] Y. Yang, M. Liu, X. You, Y. Li, H. Lin, J.P. Chen, A novel bimetallic Fe-Cu-CNT catalyst for effective catalytic wet peroxide oxidation: reaction optimization and mechanism investigation, Chem. Eng. J. 479 (2024), https://doi.org/10.1016/j.cej.2023.147320.
[20] S. Ziembowicz, M. Kida, Limitations and future directions of application of the Fenton-like process in micropollutants degradation in water and wastewater treatment: a critical review, Chemosphere 296 (2022), https://doi.org/10.1016/j.chemosphere.2022.134041.
[21] S. Zuo, S. Zhu, J. Wang, W. Liu, J. Wang, Boosting Fenton-like reaction efficiency by co-construction of the adsorption and reactive sites on N/O co-doped carbon, Appl. Catal. B 301 (2022) 120783, https://doi.org/10.1016/j.apcatb.2021.120783.
[22] Y. Ren, L. Lin, J. Ma, J. Yang, J. Feng, Z. Fan, Sulfate radicals induced from peroxymonosulfate by magnetic ferrospinel MFe_2O_4 (M = Co, Cu, Mn, and Zn) as heterogeneous catalysts in the water, Appl. Catal. B 165 (2015) 572–578, https://doi.org/10.1016/j.apcatb.2014.10.051.
[23] Y. Yang, H. Zhang, H. Huang, Y. Yan, X. Zhang, Degradation of m-cresol over iron loaded carbon nanotube microfibrous composite: kinetic optimization and deactivation study, Sep. Purif. Technol. 262 (2021), https://doi.org/10.1016/j.seppur.2021.118340.
[24] Y. Yang, H. Lin, Y. Long, Y. Mei, J.P. Chen, Development of catalytic zero-valent iron incorporated PAN catalytic film for efficient degradation of organic matters, NPJ Clean Water 7 (2024), https://doi.org/10.1038/s41545-024-00333-6.
[25] Y. Yang, S. Tang, H. Lin, H. Fu, Y. Mei, Y. Long, Catalytic reaction intensification by a novel cryogenic auxiliary synthesized Fe-PAN membrane, Ind. Eng. Chem. Res. 62 (2023) 20677–20688, https://doi.org/10.1021/acs.iecr.3c03497.
[26] A. Santos Silva, M. Seitovna Kalmakhanova, B. Kabykenovna Massalimova, J. G. Sgorlon, D.de T. Jose Luis, H.T. Gomes, Wet peroxide oxidation of paracetamol using acid activated and Fe/Co-pillared clay catalysts prepared from natural clays, Catalysts 9 (2019) 705, https://doi.org/10.3390/catal9090705.
[27] S.M. Reimbaeva, B.K. Massalimova, M.S. Kalmakhanova, New pillared clays prepared from different deposits of kazakhstan, Mater. Today Proc. 31 (2020) 607–610, https://doi.org/10.1016/j.matpr.2020.07.532.
[28] J. Wang, J. Tang, Fe-based Fenton-like catalysts for water treatment: preparation, characterization and modification, Chemosphere 276 (2021) 130177, https://doi.org/10.1016/j.chemosphere.2021.130177.
[29] H.T. Gomes, S.M. Miranda, M.J. Sampaio, J.L. Figueiredo, A.M.T. Silva, J.L. Faria, The role of activated carbons functionalized with thiol and sulfonic acid groups in catalytic wet peroxide oxidation, Appl. Catal. B 106 (2011) 390–397, https://doi.org/10.1016/j.apcatb.2011.05.044.
[30] R.S. Ribeiro, A.M.T. Silva, J.L. Figueiredo, J.L. Faria, H.T. Gomes, The influence of structure and surface chemistry of carbon materials on the decomposition of hydrogen peroxide, Carbon NY 62 (2013) 97–108, https://doi.org/10.1016/j.carbon.2013.06.001.
[31] A. Shetty, V. Molahalli, A. Sharma, G. Hegde, Biomass-derived carbon materials in heterogeneous catalysis: a step towards sustainable future, Catalysts 13 (2023), https://doi.org/10.3390/catal13010020.
[32] F.F. Roman, J.L. Diaz de Tuesta, F.K.K. Sanches, A.S. Silva, P. Marin, B.F. Machado, P. Serp, M. Pedrosa, A.M.T. Silva, J.L. Faria, H.T. Gomes, Selective denitrification of simulated oily wastewater by oxidation using Janus-structured carbon nanotubes, Catal. Today 420 (2023) 114001, https://doi.org/10.1016/j.cattod.2023.01.008.
[33] H. Steldinger, A. Esposito, K. Brunnengräber, J. Gläsel, B.J.M. Etzold, Activated carbon in the third dimension—3D printing of a tuned porous carbon, Adv. Sci. 6 (2019) 1–9, https://doi.org/10.1002/advs.201901340.
[34] A. Henrique, H. Steldinger, J.L.D. de Tuesta, J. Gläsel, A.E. Rodrigues, H.T. Gomes, B.J.M. Etzold, J.A.C. Silva, Separation of alkane isomers in a hierarchically structured 3D-printed porous carbon monolith, Chem. Eng. J. 472 (2023) 145138, https://doi.org/10.1016/j.cej.2023.145138.
[35] S. Guo, M. Chen, L. You, Y. Wei, C. Cai, Q. Wei, H. Zhang, K. Zhou, 3D printed hierarchically porous zero-valent copper for efficient pollutant degradation through peroxymonosulfate activation, Sep. Purif. Technol. 305 (2023), https://doi.org/10.1016/j.seppur.2022.122437.

[36] S. Guo, M. Chen, Y. Wei, L. You, C. Cai, Q. Wei, K. Zhou, Designing hierarchically porous zero-valent iron via 3D printing to degrade organic pollutants by activating peroxymonosulfate using high-valent iron-oxo species, Chem. Eng. J. 476 (2023), https://doi.org/10.1016/j.cej.2023.146523.
[37] J.F. Rangel-Sequeda, M. Loredo-Cancino, V.I. Águeda Maté, D.A. De Haro-Del Rio, N.E. Dávila-Guzmán, 3D printing of powdered activated carbon monoliths: Effect of structuring on physicochemical and mechanical properties and its influence on the adsorption performance, Mater. Today Commun. 33 (2022), https://doi.org/10.1016/j.mtcomm.2022.104758.
[38] P. Blyweert, J. Restivo, O.S.G.P. Soares, V. Nicolas, V. Fierro, M.F.R. Pereira, A. Celzard, First insight into the catalytic activity of stereolithographically 3D-printed tannin-based carbon architectures, ChemCatChem (2024), https://doi.org/10.1002/cctc.202400190.
[39] J.L. Diaz de Tuesta, A.M.T. Silva, J.L. Faria, H.T. Gomes, Removal of Sudan IV from a simulated biphasic oily wastewater by using lipophilic carbon adsorbents, Chem. Eng. J. 347 (2018) 963–971, https://doi.org/10.1016/j.cej.2018.04.105.
[40] A.S. Silva, J.L. Diaz de Tuesta, T. Sayuri Berberich, S. Delezuk Inglez, A.R. Bertão, I. Çaha, F.L. Deepak, M. Bañobre-López, H.T. Gomes, Doxorubicin delivery performance of superparamagnetic carbon multi-core shell nanoparticles: pH dependence, stability and kinetic insight, Nanoscale 14 (2022) 7220–7232, https://doi.org/10.1039/D1NR08550F.
[41] S. Moretto, A. Santos Silva, J.L. Diaz de Tuesta, F.F. Roman, R. Cortesi, A.R. Bertão, M. Bañobre-López, M. Pedrosa, A.M.T. Silva, H.T. Gomes, Comprehensive characterization and development of multi-core shell superparamagnetic nanoparticles for controlled delivery of drugs and their kinetic release modelling, Mater. Today Chem. 33 (2023) 101748, https://doi.org/10.1016/j.mtchem.2023.101748.
[42] B. Huang, C.H. Bartholomew, B.F. Woodfield, Improved calculations of pore size distribution for relatively large, irregular slit-shaped mesopore structure, Microporous Mesoporous Mater. 184 (2014) 112–121, https://doi.org/10.1016/j.micromeso.2013.10.008.
[43] J.L. Figueiredo, M.F.R. Pereira, The role of surface chemistry in catalysis with carbons, Catal. Today 150 (2010) 2–7, https://doi.org/10.1016/j.cattod.2009.04.010.
[44] D.R. Lima, A. Hosseini-Bandegharaei, P.S. Thue, E.C. Lima, Y.R.T. de Albuquerque, G.S. dos Reis, C.S. Umpierres, S.L.P. Dias, H.N. Tran, Efficient acetaminophen removal from water and hospital effluents treatment by activated carbons derived from Brazil nutshells, Colloids Surf. A Physicochem. Eng. Asp. 583 (2019) 123966, https://doi.org/10.1016/j.colsurfa.2019.123966.
[45] Y. Huaccallo-Aguilar, J.L. Diaz de Tuesta, S. Álvarez-Torrellas, H.T. Gomes, M. Larriba, G. Ovejero, J. García, New insights on the removal of diclofenac and ibuprofen by CWPO using a magnetite-based catalyst in an up-flow fixed-bed reactor, J. Environ. Manage. 281 (2021), https://doi.org/10.1016/j.jenvman.2020.111913.
[46] J.L. Diaz de Tuesta, A. Quintanilla, D. Moreno, V.R. Ferro, J.A. Casas, Simulation and optimization of the CWPO process by combination of aspen plus and 6-factor doehlert matrix: towards autothermal operation, Catalysts 10 (2020) 548, https://doi.org/10.3390/catal10050548.
[47] M. Thommes, K. Kaneko, A.V. Neimark, J.P. Olivier, F. Rodriguez-Reinoso, J. Rouquerol, K.S.W. Sing, Physisorption of gases, with special reference to the evaluation of surface area and pore size distribution (IUPAC Technical Report), Pure Appl. Chem. 87 (2015) 1051–1069, https://doi.org/10.1515/pac-2014-1117.
[48] N.G. González, S. Larrégola, F. Pereira, L.E. Cadus, M.R. Morales, Surface acid functionalization of activated carbons and its influence on the copper-support interactions, MDPI AG (2022) 6, https://doi.org/10.3390/eccs2021-11041.
[49] B. Hasse, J. Gläsel, A.M. Kern, D.Y. Murzin, B.J.M. Etzold, Preparation of carbide-derived carbon supported platinum catalysts, Catal. Today 249 (2015) 30–37, https://doi.org/10.1016/j.cattod.2014.10.049.
[50] P. Battistoni, S. Bompadre, G. Fava, Commercial activated carbon acidified by nitric acid oxidation. Effect of particle and pore size on the production of surface oxide structures, Mater. Chem. Phys. 11 (1984) 339–350, https://doi.org/10.1016/0254-0584(84)90038-5.
[51] S. Biniak, G. Szymański, J. Siedlewski, A. Świątkowski, The characterization of activated carbons with oxygen and nitrogen surface groups, Carbon NY 35 (1997) 1799–1810, https://doi.org/10.1016/S0008-6223(97)00096-1.
[52] A. Álvarez, M. Borges, J.J. Corral-Pérez, J.G. Olcina, L. Hu, D. Cornu, R. Huang, D. Stoian, A. Urakawa, CO_2 activation over catalytic surfaces, ChemPhysChem 18 (2017) 3135–3141, https://doi.org/10.1002/cphc.201700782.
[53] A. Taurbekov, A. Abdisattar, M. Atamanov, M. Yeleuov, C. Daulbayev, K. Askaruly, B. Kaidar, Z. Mansurov, J. Castro-Gutierrez, A. Celzard, V. Fierro, T. Atamanova, Biomass derived high porous carbon via CO_2 activation for supercapacitor electrodes, J. Compos. Sci. 7 (2023), https://doi.org/10.3390/jcs7100444.
[54] V. Thapliyal, M.E. Alabdulkarim, D.R. Whelan, B. Mainali, J.L. Maxwell, A concise review of the Raman spectra of carbon allotropes, Diam. Relat. Mater. 127 (2022) 109180, https://doi.org/10.1016/j.diamond.2022.109180.
[55] D. Prokić, M. Vukćević, A. Mitrović, M. Maletić, A. Kalijadis, I. Janković-Častvan, T. Đurkić, Adsorption of estrone, 17β-estradiol, and 17α-ethinylestradiol from water onto modified multi-walled carbon nanotubes, carbon cryogel, and carbonized hydrothermal carbon, (n.d.). https://doi.org/10.1007/s11356-021-15970-4/Published.
[56] P. Sun, Y. Hua, J. Zhao, C. Wang, Q. Tan, G. Shen, Insights into the mechanism of hydrogen peroxide activation with biochar produced from anaerobically digested residues at different pyrolysis temperatures for the degradation of BTEXS, Sci. Total Environ. 788 (2021) 147718, https://doi.org/10.1016/j.scitotenv.2021.147718.
[57] M. Martin-Martinez, B.F. Machado, P. Serp, S. Morales-Torres, A.M.T. Silva, J. L. Figueiredo, J.L. Faria, H.T. Gomes, Carbon nanotubes as catalysts for wet peroxide oxidation: the effect of surface chemistry, Catal. Today 357 (2020) 332–340, https://doi.org/10.1016/j.cattod.2019.03.014.
[58] Y. Sun, P. Zhou, P. Zhang, S. Meng, C. Zhou, Y. Liu, H. Zhang, Z. Xiong, X. Duan, B. Lai, New insight into carbon materials enhanced Fenton oxidation: a strategy for green iron(III)/iron(II) cycles, Chem. Eng. J. 450 (2022), https://doi.org/10.1016/j.cej.2022.138423.
[59] Y. Chen, W. Ren, T. Ma, N. Ren, S. Wang, X. Duan, Transformative removal of aqueous micropollutants into polymeric products by advanced oxidation processes, Environ. Sci. Technol. 58 (2024) 4844–4851, https://doi.org/10.1021/acs.est.3c06376.
[60] H. Lu, Z. Zhu, H. Zhang, J. Zhu, Y. Qiu, L. Zhu, S. Küppers, Fenton-like catalysis and oxidation/adsorption performances of acetaminophen and arsenic pollutants in water on a multimetal Cu–Zn–Fe-LDH, ACS Appl. Mater. Interfaces 8 (2016) 25343–25352, https://doi.org/10.1021/acsami.6b08933.
[61] M.R. Carrasco-Díaz, E. Castillejos-López, A. Cerpa-Naranjo, M.L. Rojas-Cervantes, On the textural and crystalline properties of Fe-carbon xerogels. Application as Fenton-like catalysts in the oxidation of paracetamol by H_2O_2, Microporous Mesoporous Mater. 237 (2017) 282–293, https://doi.org/10.1016/j.micromeso.2016.09.035.
[62] J.L. Diaz de Tuesta, A. Quintanilla, J.A. Casas, J.J. Rodriguez, Kinetic modeling of wet peroxide oxidation with a carbon black catalyst, Appl. Catal. B 209 (2017) 701–710, https://doi.org/10.1016/j.apcatb.2017.03.031.
[63] J.L. Diaz de Tuesta, A. Quintanilla, J.A. Casas, S. Morales-Torres, J.L. Faria, A.M. T. Silva, H.T. Gomes, The pH effect on the kinetics of 4-nitrophenol removal by CWPO with doped carbon black catalysts, Catal. Today 356 (2020) 216–225, https://doi.org/10.1016/j.cattod.2019.08.033.
[64] M. Forouzesh, A. Ebadi, A. Aghaeinejad-Meybodi, Continuous fixed-bed oxidation of metronidazole by the sulfate radical based process over nitric acid treated granular activated carbon, J. Water Process Eng. 36 (2020), https://doi.org/10.1016/j.jwpe.2020.101280.
[65] R.S. Ribeiro, O. Vieira, R. Fernandes, F.F. Roman, J.L. Diaz de Tuesta, A.M.T. T. Silva, H.T. Gomes, Synthesis of low-density polyethylene derived carbon nanotubes for activation of persulfate and degradation of water organic micropollutants in continuous mode, J. Environ. Manage. 308 (2022) 114622, https://doi.org/10.1016/j.jenvman.2022.114622.